ChemComm

Accepted Manuscript

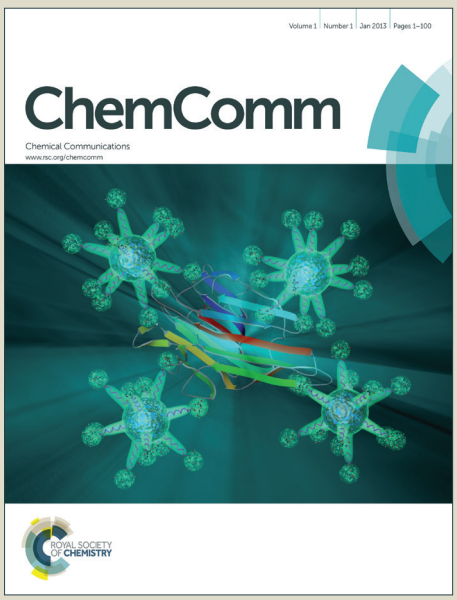

ROYAL SOCIETY OF CHEMISTRY

www.rsc.org/chemcomm

Journal Name ChemComm Dynamic Article Links ►

Cite this: DOI: 10.1039/c0xx00000x

www.rsc.org/xxxxxx

COMUNICTION

Self-assembly of Octachloroperylene Diimide into 1D Rods and 2D Plates by Manipulating the Growth Kinetic for Waveguide Applications

Huiying Liu[a,b], Xinqiang Cao[a,b], Yishi Wu[a*], Qing Liao[a], Ángel J. Jiménez,[c] Frank Würthner[c]*, and Hongbing Fu[a]*

Received (in XXX, XXX) Xth XXXXXXXXX 20XX, Accepted Xth XXXXXXXXX 20XX
DOI: 10.1039/b000000x

One-dimensional (1D) rods and 2D hexagonal plates of octachloroperylene diimide (Cl_8-PTCDI) have been selectively prepared by controlling the growth kinetic processes. Both ensemble and single-particle spectroscopy clarifies that 1D rods and 2D plates show shape dependent optical waveguiding properties.

Self-assembly of organic π-conjugated molecules into micro- and nanostructures has drawn much attention in recent years because of their wide applications in optoelectronic nano-devices.[1] Many efforts have been focused on the shape control, because the properties and performance of organic nanostructures depend not only on supramolecular organization ("packing") of the molecules, but also on the macroscopic dimensions. Accordingly, directional growth induced by "supramolecular synthons"[2] direct the orientation in the microcrystals, resulting in anisotropy of the function such as crystal-plane-dependent photoluminescence[3] and anisotropic charge transport in field effect transistor[4]. Ensuring that molecules assemble in a specific motif and form organic crystals with desired morphology, size and function, yet, remains challenging, in contrast to that of their inorganic counterparts.[5]

As one of the archetype organic semiconductor materials, perylene - 3,4:9,10 - tetracarboxylic diimide derivatives (PTCDIs)[6] have attracted great interest due to their exceptional stability, excellent optical properties and promising wide-ranging applications in optoelectronic devices such as field effect transistors,[7] waveguides,[8] and solar cells.[9] Moreover, PTCDIs exhibit strong π-π stacking interactions between the PTCDI cores, which make them ideal candidates for the investigating of solid-state molecular packing effects. Different shapes of PTCDIs could already be prepared, such as 0D particles,[10] 1D belts /rods[11] and 2D plates.[12] However, to the best of our knowledge, self-assembly of a single PTCDI compound into different nanostructures has not yet been explored, in spite of its great importance in understanding of the relationship between molecular packing and optoelectronic properties.

Herein, we report a facile solution-growth method to generate well defined 1D rods and 2D plates of a PTCDI derivative by controlling the growth kinetics. For our studies we chose a special PTCDI derivative, i.e. Cl_8-PTCDI whose solid state packing is governed not only by π–π-stacking interactions but additionally by hydrogen-bonds between the imide functionalities, leading to a unique 2D brickstone-type packing arrangement.[13]

By subtle choice of the crystal growth conditions distinct crystal shapes became available, driven by modulation of the growth kinetic along π-π stacking and hydrogen bonding interaction directions. Moreover, single-particle spectroscopy demonstrated that 1D rods and 2D plates show shape-dependent optical waveguide properties, suggesting potential applications in optoelectronic devices.

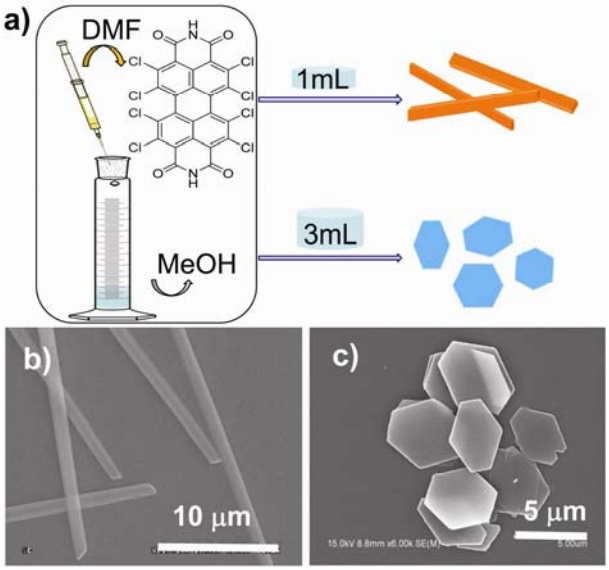

Fig. 1 a) The self-assembly of dimensionally-confined Cl_8-PTCDI structures 1D rods and 2D plates. b) and c) SEM images of Cl_8-PTCDI 1D rods and 2D plates. The scale bars are labelled in the images.

The molecule Cl_8-PTCDI was synthesized and purified as previously described.[13] Two distinct nanostructures of Cl_8-PTCDI, i.e., well-defined 1D rods and 2D plates, were prepared via a facile self-assembly protocol using the biphasic solvent methods (dimethyl formamide and methanol). In a typical preparation, 200 μL of 2.2 mM Cl_8-PTCDI solution in DMF was injected into varying volumes of methanol (V_{MeOH}). The turbulent mixing of DMF and methanol changes the solubility of the molecules and solvent polarity, thus inducing the nucleation and growth of Cl_8-PTCDI nanostructures. The shape of Cl_8-PTCDI nanostructures significantly altered by adjusting the value of V_{MeOH}, for example, 1D rods at V_{MeOH} = 1 mL in one hour and 2D plates at V_{MeOH} = 3 mL over ten hours (Fig. 1a). The as-prepared 1D rods have a

rectangular cross-section with a width of 0.5-2 μm and a length of 20-50 μm determined by SEM images (Fig. 1b and S1a), and a thickness of 300 ± 80 nm as revealed by images of atom force microscopy (AFM, Fig. S2a). And most of 2D plates generally have a hexagonal shape with an edge length of 3-10 μm (Fig. 1c and Fig. S2b) and a thickness range from 0.6 to 1.5 μm (Fig. S2b).

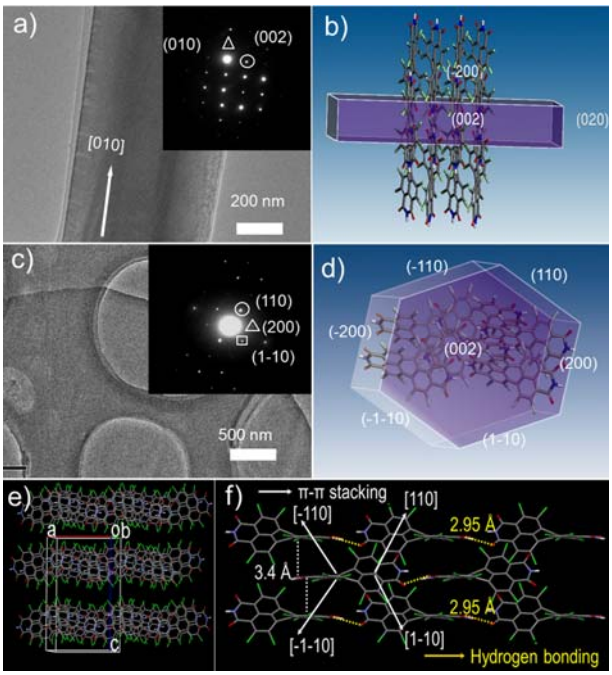

Fig. 2 a) and c) TEM images of 1D rod and 2D plate Inset: SAED pattern. b) and d) Schematic model for the 1D rod and 2D plate. e) Molecular structure of Cl_8-PTCDI in crystal, packing arrangement by viewing onto the *a,c* plane f) Front view of molecular arrangement onto the *a,b* plane.

To investigate the packing arrangement of Cl_8-PTCDI molecules within 1D rods and 2D plates, selected-area electron diffraction (SAED) and X-ray diffraction (XRD) measurements were carried out. On the basis of the orthorhombic single-crystal data of Cl_8-PTCDI,[13] both 1D rods and 2D plates belong to the cell parameters of a = 14.455(2) Å, b = 7.3585(13) Å, c = 20.033(3) Å, $\alpha = \beta = \gamma = 90°$. The circled and triangled sets of SAED spots, shown in the inset of Fig. 2a for 1D rods, are due to Bragg reflections from {002} and {010} crystal planes with *d*-spacing values of 10 and 7.4 Å, respectively. The SAED spots indicated that the rods were single-crystalline, growing along the crystal [010] direction (Fig. 2a). It can be seen from Figure. 3 that the XRD spectrum of 1D rods (blue curve), while indicates the relative abundance of (100) facets on the surfaces of 1D rods. Based on SAED and XRD results together, we draw a schematic model for 1D rods in Fig. 2b. The flat top- and bottom-faces of 1D rods are bounded by (200) crystal planes, while the side-faces are bounded by (002) crystal planes. Therefore, Cl_8-PTCDI molecules in 1D rods stand perpendicular to the substrate exposed imide groups toward the top- and bottom-faces.

In contrast to 1D rods, hexagonal plates of Cl_8-PTCDI exhibit a 2D growth. In the inset of Fig. 2c, the circled and squared sets of SAED spots are ascribed to reflections from (110)s and (1-10)s crystal planes with a *d*-spacing value of 6.6 Å, while the triangled set of spots is due to (200) crystal planes with a *d*-spacing value of 7.2 Å. Additional XRD pattern (red curve in Fig. 3) has validated the single-crystalline nature of 2D plates. The diffraction peaks ascribed to (002), (004), (006) and (008) explicitly suggests that 2D plates adopt a lamellar structure along crystal *c*-axis (Fig. 2e). Fig. 2d draws a schematic model for hexagonal plates, of which Cl_8-PTCDI molecules in hexagonal plates lie parallel to the substrate, rather than perpendicular to the substrate in 1D rods (Fig. 2b). Fig. 2f depicts the molecular arrangement of Cl_8-PTCDI within the (002) crystal plane. As one can see, this brickstone packing mode of twisted Cl_8-PTCDI molecules exhibits π-π stacking interactions with a separation of 3.4 Å along [110]s directions (white arrows), as well as hydrogen-bonding intermolecular contacts (yellow dashed lines) along the crystal [200] direction. Therefore, the 2D-growth of Cl_8-PTCDI plate demonstrates a synergistic effect between hydrogen bonding and π-π stacking interactions. This is different from 1D rods, which show growth along the [010] direction (i.e., a sum of [110] and [-110]) driven by π–π interactions.

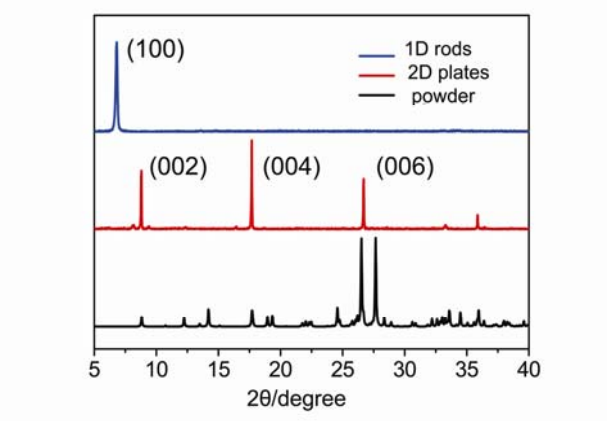

Fig. 3 X-ray diffraction patterns of Cl_8-PTCDI 1D rods (blue), 2D plates (red) and simulated powder pattern using Mercury software (black)

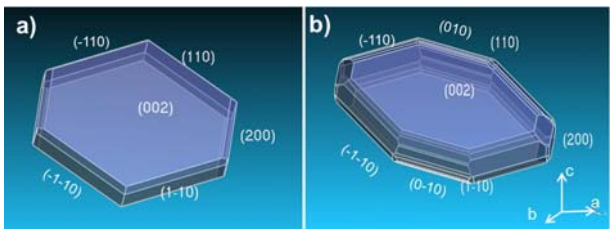

Fig. 4 a) The predicted growth morphology of Cl_8-PTCDI based on the attachment energies. b) The equilibrium shape for minimum total surface energy, calculated by the software of Materials Studio package.

Further insights into the microcrystal self-assembly have been given by our calculation results using Material Studio package (Fig 4 and Table 1). The growth morphology predicted based on the attachment energies[14] is an analogy of hexagonal plate (Fig. 4a), while the equilibrium shape for minimum total surface energy[15] exhibits as an octagonal plate (Fig. 4b). In any event, both growth and equilibrium shapes are mainly bounded by the lowest-energy (002)s crystal faces (Table1). This suggests that hexagonal plates of of Cl_8-PTCDI obtained at V_{MeOH} = 3mL in our experiments is the thermodynamically stable one, while 1D rods obtained at V_{MeOH} = 1 mL represents a metastable but kinetically favored high-energy state. This is further verified by the Ostwald ripening experiment, in which as-formed 1D-rods were found to transform into 2D plate-like structures after kept in

the pristine DMF/MeOH for five days (Fig S3). In this process the high surface energy of 1D-rods bounded by both (200) and (020) crystal facets promotes their re-dissolution, whereas material is re-deposited on low surface energy of plates bounded mainly by (002) crystal plane.

Table 1 Surface free and attachment energies of various crystal facets (*hkl*) calculated by using the material studio package

Miller Index{*hkl*}	d_{hkl} (Å)	$\gamma_{\{hkl\}}$(kcal/mol)	$E^{attach}_{\{hkl\}}$ (kcal/mol)
{002}s	10.0	16.9	-67.6
{020}s	3.7	58.5	-200.9
{200}s	7.2	63.7	-213.9
{110}s	6.5	78.6	-155.2

In our experiments, the value of V_{MeOH} were changed to adjust the Cl_8-PTCDI concentration of C, consequently, the supersaturation ($\sigma = C/C_{equilibrium}$) [14b]. Generally, the driving force for crystallization can be expressed as $\Delta\mu = k_BT\ln(\sigma)$, where $\Delta\mu$ is the difference in chemical potential between Cl_8-PTCDI molecules in the crystal and the liquid phase, k_B is the Boltzmann's constant, T is the absolute temperature[16]. Note that both attachment and surface energy theories do not consider the driving force of $\Delta\mu/k_BT$. This might be responsible for the inconsistency of the predicted growth morphology (Fig. 4a) with the observed 1D-rods at high supersaturation. In consideration of the driving force for crystallization, the most widely-accepted crystal growth mechanisms are two-dimensional (2D) nucleation and spiral growth[16-18]. According to these two mechanisms, the relative growth rate $R_{\{hkl\}}$ of the crystal faces {*hkl*} was given by

$$R_{\{hkl\}} \propto C \times \exp(-\Delta G^{\neq}_{\{hkl\}} / k_BT) \qquad (1)$$

where C is the concentration of Cl_8-PTCDI, and $\Delta G^{\neq}_{\{hkl\}}$ is the activation free energy of the crystal face {*hkl*}. Generally, the kinetic barrier is inversely proportional to the surface energy.[17] According to the calculated surface energies order: $\gamma_{\{002\}s} < \gamma_{\{020\}s} < \gamma_{\{200\}s} < \gamma_{\{110\}s}$ (Table 1), as a consequence, the value of $\Delta G^{\neq}_{\{hkl\}}$ might follow the order: $\Delta G^{\neq}_{\{110\}} < \Delta G^{\neq}_{\{200\}} < \Delta G^{\neq}_{\{020\}} < \Delta G^{\neq}_{\{002\}}$. It is well known that the relative growth rates of $R_{\{hkl\}}$ depends on the kinetic barriers $\Delta G^{\neq}_{\{hkl\}}$. At low supersaturation (V_{MeOH} = 3 mL), the hexagonal plates are obtained, it is most likely because the chemical potential ($\Delta\mu$) of this system is high enough to overcome the barrier of $\Delta G^{\neq}_{\{200\}}$, giving $\Delta G^{\neq}_{\{002\}} > \Delta G^{\neq}_{\{020\}} > \Delta\mu \geq \Delta G^{\neq}_{\{200\}} > \Delta G^{\neq}_{\{110\}s}$. Therefore, the rapid growth of {110}s, {1-10}s, {-110}s,{-1-10}s faces and {200}s, {-200}s result in the crystallization toward hexagonal shape bounded mainly by low surface energy{002}s facets, yielding a thermodynamically favorable shape. On the other hand, at high supersaturation (V_{MeOH} = 1 mL), the chemical potential of the system ($\Delta\mu$) is increased high enough to overcome the growth barrier of $\Delta G^{\neq}_{\{020\}}$, making $\Delta G^{\neq}_{\{002\}} > \Delta\mu \geq \Delta G^{\neq}_{\{020\}}$. As a result, the products obtained from high supersaturation prefer 1D growth along [020] direction with the exposed on (002)s and (200)s faces, giving a kinetic favored product with high energy.

The optical waveguide properties of 1D rods and 2D plates were investigated by near-field scanning optical microscopy (NSOM, Fig S4). The spatially resolved PL spectra in Fig. 5 demonstrate the out-coupled emission and confirm the self-guiding properties. As shown in Fig. 5a and b, the emission collected from the edge (black dash line) is slightly red-shifted by about 10 nm compared to that of laser spot (red solid line) due to re-absorption of waveguided light during propagation resulting from the overlap between the absorption and PL emission (Fig S5). It was anticipated that the direction of waveguiding propagation should be confined by the boundary of crystal morphology. When the laser beam excited only the central part of the 1D rod, propagation of the light to both tips was observed (inset of Fig. 5a). Moreover, when the laser was focused at the center of a 2D plate, propagation of waveguided light was allowed to spread in all the horizontal direction (Fig S6). Upon moving the excited spot to one of the corners of a 2D plate propagation of the light to the diagonal edges was observed (inset of Fig. 5b). Therefore, the confinement of 1D or 2D morphology leads to the confinement of the propagated light, demonstrating shape-dependent optical waveguiding behaviour.

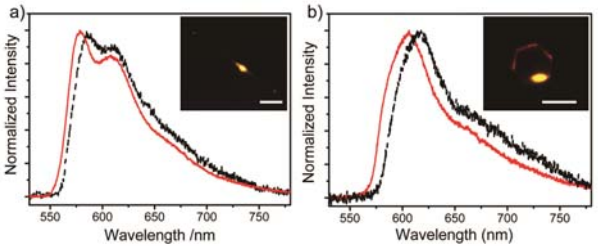

Fig. 5 Normalized emission spectra of micro-area: a) 1D rod and b) 2D plate, collected by NSOM from the laser spot (red) and the edge of particles (black) separately. The excitation wavelength is 471 nm. Insert: Dark-field PL images of microcrystals, with the scale bar of 10 μm.

In summary, 1D rods and 2D plates of Cl_8-PTCDI were obtained by controlling the growth process. Structural analyses have revealed the favored growth directions which are along the π–π-stacking direction in 1D rods and along both π–π-stacking and hydrogen-bonding directions in 2D plates. Surface energy calculations reveal that 1D rods represent an only metastable but kinetically favored high-energy state, while 2D plates are a result of the thermodynamically most stable shape with lowest surface energy. Furthermore, the 1D rods show waveguiding along the 1D direction and 2D plates give rise to the waveguide within the 2D plane. The present results of controllable morphology of Cl_8-PTCDI microcrystals might further pave the way for potential application of organic small molecules in optoelectronic devices.

This work was supported by National Natural Science Foundation of China (Nos. 20925309, 21190034, 21221002) and the National Research Fund for Fundamental Key Project 973 (2011CB808402, 2013CB933500).

Notes and references

[a] *Beijing National Laboratory for Molecular Science (BNLMS), Institute of Chemistry, Chinese Academy of Sciences, Beijing 100190, P. R. China; Fax: +86-10-82616517; Tel: +86-10-62526801*
E-mail: hongbing.fu@iccas.ac.cn;
[b] *Graduate University of Chinese Academy of Sciences (GUCAS), Beijing 100049, P.R.China*

[c] *Universität Würzburg, Institut für Organische Chemie and Röntgen Research Center for Complex Material Systems Am Hubland, 97074 Würzburg (Germany) Fax: +49 931-3184756; Tel: +49-931-3185340 E-mail: wuerthner@chemie.uni-wuerzburg.de*

†Electronic Supplementary Information (ESI) available: Experimental details, detailed experimental setup and more morphology characteristic measurements. See DOI: 10.1039/b000000x/

1. (a) N. Chandrasekhar and R. Chandrasekar, *Angew. Chem. Int. Ed.*, 2012, **51**, 3556-3561. (b) C. Wang, Y. Liu, Z. Ji, E. Wang, R. Li, H. Jiang, Q. Tang, H. Li and W. Hu, *Chem. Mater.*, 2009, **21**, 2840-2845. (c) B. Dong, T. Sakurai, Y. Honsho, S. Seki and H. Maeda, *J. Am. Chem. Soc.*, 2013, **135**, 1284-1287. (d) C.-C. Chu, G. Raffy, D. Ray, A. D. Guerzo, B. Kauffmann, G. Wantz, L. Hirsch and D. M. Bassani, *J. Am. Chem. Soc.*, 2010, **132**, 12717-12723. (e) F. S. Kim, G. Ren and S. A. Jenekhe, *Chem. Mater.*, 2010, **23**, 682. (f) G. Ren, E. Ahmed and S. A. Jenekhe, *J. Mater. Chem.*, 2012, **22**, 24373
2. G. R. Desiraju, *Angew. Chem. Int. Ed.,* 1995, **34**, 2311-2327.
3. J. E. Park, M. Son, M. Hong, G. Lee and H. C. Choi, *Angew. Chem. Int. Ed.*, 2012, **51**, 1-7.
4. (a) T. He, X. Zhang, J. Jia, Y. Li and X. Tao, *Adv. Mater.*, 2012, **24**, 2171-2175; (b) A. Lv, Y. Li, W. Yue, L. Jiang, H. Dong, G. Zhao, Q. Meng, W. Jiang, Y. He, Z. Li, Z. Wang and W. Hu, *Chem. Commun.*, 2012, **48**, 5154-5156.
5. P. Jonkheijm, P. van der Schoot, A. Schenning and E. W. Meijer, *Science*, 2006, **313**, 80-83.
6. (a) F. Wurthner, *Chem. Commun.*, 2004, **0**, 1564-1579; (b) C. Huang, S. Barlow and S. R. Marder, *J. Org. Chem.*, 2011, **76**, 2386-2407. T. W. Chamberlain, E. S. Davies, A. N. Khlobystov and N. R. Champness, *Chem. Eur. J.*, 2011, **17**, 3759-3767.
7. (a) J. Jang, S. Nam, D. S. Chung, S. H. Kim, W. M. Yun and C. E. Park, *Adv. Funct. Mater.*, 2010, **20**, 2611-2618. (b) C.-C. Chu, G. Raffy, D. Ray, A. D. Guerzo, B. Kauffmann, G. Wantz, L. Hirsch and D. M. Bassani, *J. Am. Chem. Soc.*, 2010, **132**, 12717-12723.
8. Q. Bao, B. M. Goh, B. Yan, T. Yu, Z. Shen and K. P. Loh, *Adv. Mater.*, 2010, **22**, 3661-3666.
9. X. Zhan, Z. a. Tan, B. Domercq, Z. An, X. Zhang, S. Barlow, Y. Li, D. Zhu, B. Kippelen and S. R. Marder, *J. Am. Chem. Soc.*, 2007, **129**, 7246-7247.
10. K. Balakrishnan, A. Datar, T. Naddo, J. Huang, R. Oitker, M. Yen, J. Zhao and L. Zang, *J. Am. Chem. Soc.*, 2006, **128**, 7390-7398.
11. (a) Y. Che, X. Yang, G. Liu, C. Yu, H. Ji, J. Zuo, J. Zhao and L. Zang, *J. Am. Chem Soc.*, 2010, **132**, 5743-5750; (b) X. Cao, Y. Wu, H. Fu and J. Yao, *J. Phys. Chem. Lett.*, 2011, **2**, 2163-2167.
12. X. Cao, S. Bai, Y. Wu, Q. Liao, Q. Shi, H. Fu and J. Yao, *Chem. Commun.*, 2012, **48**, 6402-6404.
13. M. Gsänger, J. H. Oh, M. Könemann, H. W. Höffken, A.-M. Krause, Z. Bao and F. Würthner, *Angew. Chem. Int. Ed.*, 2010, **49**, 740-743.
14. (a) Murray, C. B.; Kagan, C. R., *Annu. Rev. Mater. Sci.*, 2000, **30**, 545-610; (b) L. Huang, Q. Liao, Q. Shi, H. Fu, J. Ma and J. Yao, *J. Mater. Chem.*, 2010, **20**, 159-166.
15. (a) S. X. M. Boerrigter, H. M. Cuppen, R. I. Ristic, J. N. Sherwood, P. Bennema and H. Meekes, *Cryst. Growth. Des.*, 2002, **2**, 357-361; (b) L. Kang, H. Fu, X. Cao, Q. Shi and J. Yao, *J. Am. Chem. Soc.*, 2011, **133**, 1895-1901.
16. (a)Y. Yin and A. P. Alivisatos, *Nature*, 2005, **437**, 664-670; (b) Sunagawa, I. Crystals: *Growth, Morphology and Perfection*; Cambridge University Press: Cambridge, 2005.
17. (a) S. Piana, M. Reyhani and J. D. Gale, *Nature*, 2005, **438**, 70-73; (b) S. M. Lee, S. N. Cho and J. Cheon, *Adv. Mater.*, 2003, **15**, 441-444; (c) G. R. Desiraju, *Nat. Mater.*, 2002, **1**, 77-79.
18. (a) X. Y. Liu, E. S. Boek, W. J. Briels and P. Bennema, *Nature*, 1995, **374**, 342-345. (b) Mullin, J. W. Crystallization, 3rd ed.; Butterworth Heinemann: Oxford, 1992; Chapter 6, pp 202-260. (c) M. A. Lovette, A. R. Browning, D. W. Griffin, J. P. Sizemore, R. C. Snyder and M. F. Doherty, *Ind Eng Chem Res*, 2008, **47**, 9812-9833.